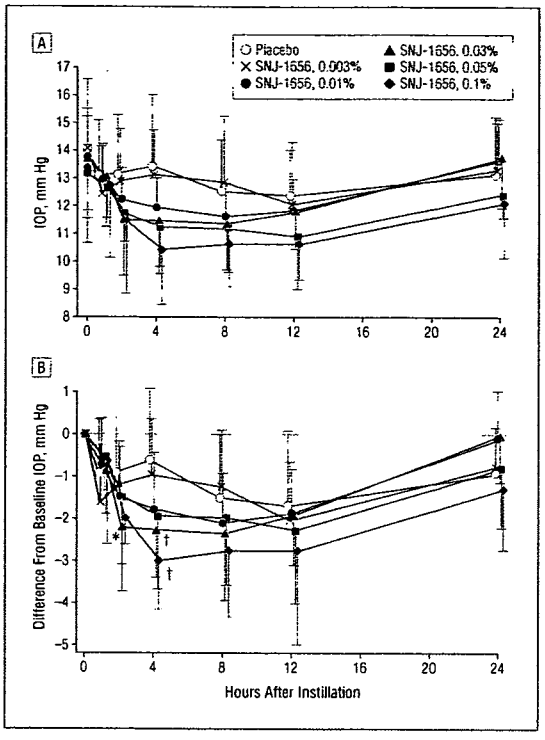

Figure 1. Levels of intraocular pressure (IOP) after single instillation of SNJ-1656. A, Levels of IOP decreased after instillation but were restored by 24 hours after instillation. B, Reduction of IOP after instillation of SNJ-1656 was dose dependent. Values are represented as mean±SD (SNJ-1656 group, 12 eyes in 6 subjects; placebo group, 30 eyes in 15 subjects). The significance of findings was evaluated by the Dunnett test (2 sided). *$P \leq .05$ compared with the placebo group. †$P \leq .01$ compared with the placebo group.

4 hours in the placebo, 0.003%, 0.01%, 0.03%, 0.05%, and 0.1% groups, respectively. Statistical analyses demonstrated significant differences in the magnitude of IOP reduction between the SNJ-1656– and placebo-treated eyes for 0.03% to 0.1% solutions ($P = .04$ at 2 hours and $P = .01$ at 4 hours for the 0.03% solution; $P < .001$ at 4 hours for the 0.1% solution [2-sided Dunnett test]) (Figure 1B). With SNJ-1656, 0.1%, mean IOP was 12.79±2.64, 11.44±2.58, 10.42±1.97, 10.63±1.56, 10.63±1.30, and 12.10±2.00 mm Hg at 1, 2, 4, 8, 12, and 24 hours after the instillation, respectively. Maximal IOP change with SNJ-1656, 0.1%, −3.00±1.16 mm Hg from the baseline IOP, was observed at 4 hours after instillation, and the IOP then slowly returned to near-baseline levels during the next 24 hours. The maximal IOP reduction after instillation of SNJ-1656, 0.1%, was larger than the reductions after instillation of lower concentrations (0.003% to 0.05%) of SNJ-1656. Similar, but weaker IOP-lowering effects were observed with lower concentrations of SNJ-1656.

SAFETY IN SINGLE-DOSE TRIAL

On slitlamp examination during the trial, there were no significant findings except hyperemia of the bulbar and palpebral conjunctiva in eyes treated with SNJ-1656 (**Figure 2**). This finding as a treatment-related adverse

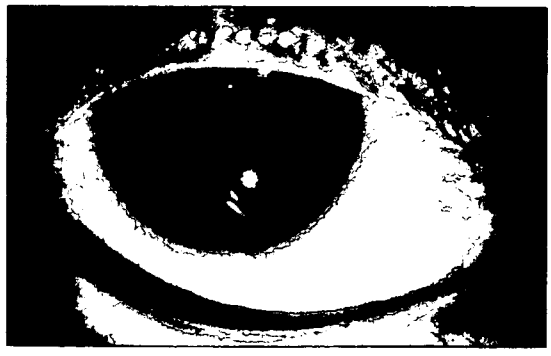

Figure 2. Bulbar conjunctival hyperemia after instillation of SNJ-1656, 0.1%.

event was achieved in all 6 eyes with instillation of the 0.1% concentration and in 5 of the 6 eyes with instillation of the 0.05% concentration (**Table 1**). One subject with ocular hyperemia caused by SNJ-1656, 0.1%, experienced blurred vision, and another treated at this dose experienced photophobia. In contrast, with the 0.003% and 0.01% concentrations of SNJ-1656, fewer incidences of ocular hyperemia occurred, and no hyperemia occurred in the placebo group. The bulbar conjunctival hyperemia disappeared in all eyes, including those receiving the 0.1% concentration of SNJ-1656 (**Table 2**), by 12 hours after the instillation. Monitoring of pupil diameter showed no significant changes in pupil size during the trial. No significant changes were found between the preinstillation and postinstillation electroretinograms or the examination findings in the ocular fundus, the corneal endothelial cell count, or the corneal thickness. In addition, physiological examination results including blood pressure, pulse, body temperature, electrocardiograms (a wave, b wave, and amplitude), and hematological and urine testing showed no significant differences among volunteers administered SNJ-1656 or placebo.

IOP-LOWERING EFFECT OF REPEATED-INSTILLATION TRIAL

In the repeated-instillation trial, once-daily administration (steps 1 and 2-1) decreased IOP levels after instillation at 9 AM on each day in the SNJ-1656– and placebo-treated eyes (**Figure 3**A), whereas such a pattern of changes in IOP was unclear with twice-daily administration (steps 2-2 and 3; Figure 3B). The change in IOP from baseline was significantly larger in eyes treated with SNJ-1656 once daily (steps 1 and 2-1; Figure 3C) or twice daily (steps 2-2 and 3; Figure 3D) than in eyes treated with placebo. The mean changes in IOP from the baseline on the seventh day were −1.86±1.93, −2.78±0.98, and −3.70±1.12 ($P = .01$, vs placebo [2-sided Dunnett test]) mm Hg at 2 hours, and −1.58±1.56, −1.87±0.93, and −4.12±1.39 ($P < .001$) mm Hg at 4 hours in the groups receiving placebo and SNJ-1656 at concentrations of 0.05% (step 1) and 0.1% (step 2-1), once daily, respectively. Changes in IOP on the seventh day were −0.92±1.32, −3.45±1.18 ($P < .001$), and −2.51±1.74 ($P = .02$) mm Hg at 2 hours, and −1.19±1.10, −2.87±1.34

Table 1. Treatment-Related Adverse Events in Single-Dose Trial of SNJ-1656[a]

Symptom/Signs	SNJ-1656 Concentration				
	0.003% (n=6)	0.01% (n=6)	0.03% (n=6)	0.05% (n=6)	0.1% (n=6)
Bulbar conjunctival hyperemia	1	0	2	5	6
Palpebral conjunctival hyperemia	1	0	0	0	0
Blurred vision	0	0	0	0	1
Photophobia	0	0	0	0	1

[a] Data are expressed as number of volunteers with reported treatment-related adverse events. No treatment-related adverse events occurred in the placebo group (n=15).

Table 2. Change in Score of Bulbar Conjunctival Hyperemia After Instillation of SNJ-1656, 0.1%, in the Single-Dose Trial[a]

Time After Instillation, h	Score		
	0	0.5	1
0	12	0	0
1	0	0	12
4	0	4	8
8	2	7	3
12	4	8	0
24	8	4	0

[a] Data are expressed as number of eyes of the 12 eyes in 6 volunteers. No eyes achieved scores of 2 or 3. Scores are described in the "Methods" section.

($P=.01$), and -2.94 ± 1.75 ($P=.01$) mm Hg at 4 hours in the groups receiving placebo and SNJ-1656 at concentrations of 0.05% (step 2-2) and 0.1% (step 3), twice daily, respectively. The IOP-lowering effects of SNJ-1656 on the seventh day were similar to those on the first day in once- or twice-daily administration. The maximal changes in IOP in the SNJ-1656 groups were observed from 2 to 4 hours after instillation.

SAFETY IN REPEATED-INSTILLATION TRIAL

Hyperemia of the bulbar and palpebral conjunctiva as a treatment-related adverse event was observed in all steps in the repeated-instillation trial (**Table 3**). Some subjects treated with SNJ-1656, 0.1% (2 volunteers in step 2-1 and 1 volunteer in step 3), experienced blurred vision. One volunteer in step 3 complained of photophobia, ocular fatigue, and dryness of the eyes. In all of the subjects with these adverse effects, ocular hyperemia and other ocular symptoms disappeared spontaneously after the cessation of SNJ-1656 instillation. The bulbar conjunctival hyperemia disappeared in all eyes, including those receiving once-daily and twice-daily SNJ-1656, 0.1% (**Table 4**), by 8 hours after the instillation. There were no significant differences in pupil diameter between SNJ-1656 and placebo administrations. In addition, there were no other abnormal findings on slitlamp examination, no other ocular symptoms, and no significant abnormal physiological findings, including those for blood pressure, pulse, body temperature, and the electrocardiograms during the trial. There were no clinically significant changes from baseline in visual acuity, ocular fundus characteristics, corneal endothelial cell count, corneal thickness, electroretinographic findings, or laboratory values (hematologic analysis, blood chemistry, or urinalysis results) after the trial in the SNJ-1656 groups.

COMMENT

The IOP-lowering effects of SNJ-1656 in healthy adult volunteers were demonstrated in this study, which included a single-dose stage and a prolonged repeated-instillation stage. The study solution SNJ-1656 is an ophthalmic solution of Y-39983, a novel selective ROCK inhibitor, which has been reported to exhibit potent IOP-reducing activity in rabbits and monkeys.[14] Our findings obtained in this single-dose trial demonstrated that SNJ-1656 at concentrations ranging from 0.003% to 0.1% reduced IOP in a dose-dependent fashion without systemic or severe local ocular adverse effects. Mean IOPs in eyes treated with SNJ-1656, 0.03%, were significantly lower from 2 to 4 hours after instillation than were IOPs in eyes treated with placebo. The repeated-instillation trial also showed that IOP reductions from baseline were significantly larger in eyes with SNJ-1656 applications once daily and twice daily than in eyes treated with placebo. Maximal IOP reduction was observed from 2 to 4 hours after the instillation of SNJ-1656. No significant systemic adverse effects were observed. In addition, because IOP returned to baseline levels by 24 hours after instillation, and statistical difference from placebo in twice-daily administration was more than that in once-daily administration, twice-daily administration of this ophthalmic solution can be recommended as clinically useful.

In both the single- and repeated-instillation trials, the subjects experienced ocular treatment-related adverse events, although no systemic adverse events were observed. In our clinical trial, the most frequent adverse event was ocular hyperemia. Most of the subjects experienced no hyperemia or trace to mild hyperemia. In all cases, ocular hyperemia was transient and disappeared spontaneously after the cessation of SNJ-1656 instillation. Because the disappearance of hyperemia was confirmed in all eyes on slitlamp examination, SNJ-1656 did not seem to pose any safety problems for patients treated with lower concentrations. The occurrence of ocular hyperemia is

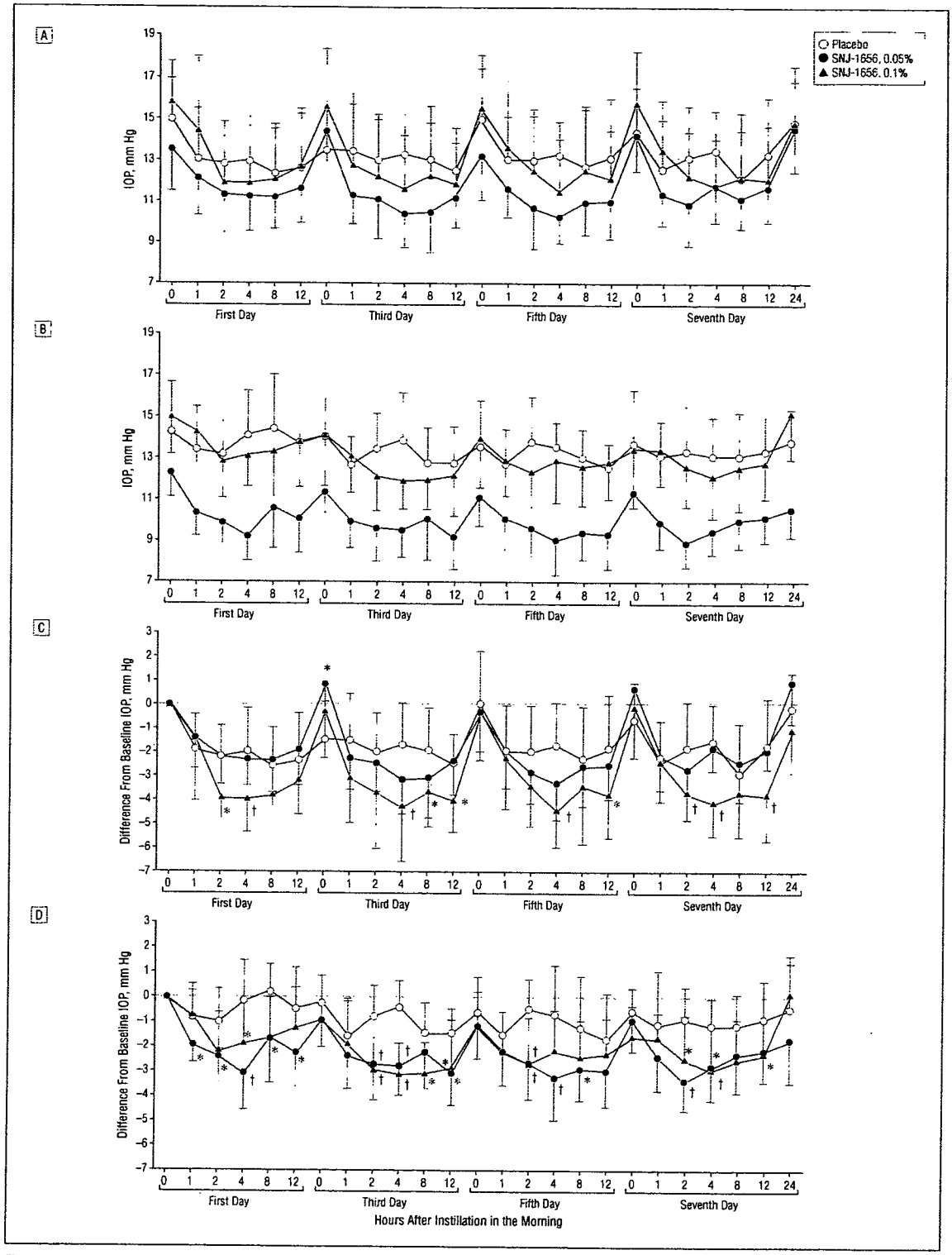

Figure 3. Levels of intraocular pressure (IOP) during repeated instillation of SNJ-1656. Levels of IOP in eyes with once-daily instillation of SNJ-1656 and placebo decreased after every 9 AM instillation (A), whereas diurnal changes in IOP were unclear with twice-daily administration (B). Reduction of IOP was significantly larger in eyes with SNJ-1656 administered once daily (C) or twice daily (D) than in eyes treated with placebo. Values are represented as mean±SD (12 eyes in 6 subjects). The significance of findings was evaluated by the Dunnett test (2 sided). *$P \leq .05$ compared with the placebo group. †$P \leq .01$ compared with the placebo group.

Table 3. Treatment-Related Adverse Events in Repeated-Instillation Trial of SNJ-1656[a]

	Once-Daily Administration (n=6)		Twice-Daily Administration (n=6)	
Symptom/Signs	SNJ-1656, 0.05%	SNJ-1656, 0.1%	SNJ-1656, 0.05%	SNJ-1656, 0.1%
Bulbar conjunctival hyperemia	2	6	5	5
Palpebral conjunctival hyperemia	1	3	3	1
Blurred vision	0	2	0	1
Photophobia	0	0	0	1
Ocular fatigue	0	0	0	1
Dryness of the eyes	0	0	0	1

[a] Data are expressed as number of volunteers with reported treatment-related adverse events. No treatment-related adverse events occurred in the placebo group.

Table 4. Change in Score of Bulbar Conjunctival Hyperemia After Instillation of SNJ-1656, 0.1%, on the Seventh Day in the Repeated-Instillation Trial[a]

Time After Instillation, h	Score 0	0.5	1
	Once-Daily Instillation		
0	12	0	0
1	0	4	8
4	3	8	1
8	9	3	0
12	12	0	0
24	12	0	0
	Twice-Daily Instillation		
0	12	0	0
1	2	4	6
4	6	6	0
8	10	2	0
12	12	0	0
24	12	0	0

[a] Data are expressed as number of eyes in the 12 eyes in 6 volunteers. No eyes achieved scores of 2 or 3. Scores are described in the "Methods" section.

consistent with findings in our previous animal experiments, in which similar conjunctival hyperemia (and minor hemorrhage) was found in rabbits and monkeys after frequent instillation of higher doses of SNJ-1656.[14] Hyperemia may be the result of relaxation of the blood vessels because ROCK inhibition induces smooth muscle relaxation.[11] Also, sporadic subconjunctival hemorrhage may be caused by impairment of barrier function or morphologic changes in vascular endothelial cells.[14] There were no clinically relevant effects of SNJ-1656 on visual acuity, ocular fundus characteristics, corneal endothelial cell count, corneal thickness, or electroretinographic findings. In addition, no clinically significant effects on blood pressure, pulse, body temperature, or electrocardiographic findings were noted with administration of SNJ-1656. The results of this study thus indicate that the IOP-lowering efficacy of SNJ-1656 was significant in healthy volunteers, and that adverse effects of its administration did not matter. Because we observed no systemic adverse effects in this study, we believe that the use of SNJ-1656 is safe, even for patients with systemic disease.

Aqueous outflow in the conventional pathway is regulated by the contraction and relaxation of the CM, and also by the TM, which possesses smooth musclelike properties.[15] It is thought that CM contraction distends the TM and increases aqueous outflow, whereas TM contraction decreases aqueous outflow.[6] Aqueous outflow is thus inversely influenced by the contractility of TM and CM. The contraction and relaxation of smooth muscle are regulated by myosin light chain phosphorylation/dephosphorylation. ROCK is involved in one of the major pathways of myosin light chain phosphorylation and is thought to regulate actomyosin-based contractility in many types of cells by phosphorylation of ROCK substrates.[16-18] Involvement of ROCK in control of IOP via regulation of the aqueous conventional outflow pathway has principally been demonstrated by 2 types of evidence: effects on the cellular behavior of TM, and the contribution of ROCK to the contractility of CM and TM. Recent studies have indicated that cytoskeletal drugs, including ROCK inhibitors, decrease aqueous outflow resistance by modulating cytoplasmic fibers.[19] In previous studies,[11,20] we found that the selective ROCK inhibitor Y-27632 causes alterations in cell shape; decreases actin stress fibers and focal adhesions in cultured human TM cells; elicits profound effects on TM cell activities, including adhesion, gel contraction, and cell motility; and decreases IOP in rabbit eyes. It has also been shown that Y-27632 increases aqueous outflow in enucleated, perfused porcine eyes[21] and that topical application of Y-39983 significantly decreases IOP in monkey eyes.[22] The inhibitors Y-27632 and Y-39983 induce relaxation of carbachol-contracted rabbit CM strips and TM[11,13] and contract monkey TM, exhibiting involvement of phosphorylation of myosin phosphatase by ROCK.[23] Collectively, these findings suggest that TM is a target for the development of new cytoskeletal drugs, including ROCK inhibitors, for new treatment of glaucoma. Based on the findings of the present study, SNJ-1656 can be considered a candidate drug for lowering IOP by increasing conventional outflow with few adverse effects.

In conclusion, our findings demonstrated that SNJ-1656 is a safe topical agent that is effective in reducing IOP in healthy adult volunteers. However, because our

trial was attempted primarily to evaluate the safety of SNJ-1656 in healthy subjects, further clinical trials will be required for elucidation of IOP-lowering effects in patients with ocular hypertension and/or primary open-angle glaucoma.

Submitted for Publication: March 18, 2007; final revision received July 31, 2007; accepted August 17, 2007.
Correspondence: Hidenobu Tanihara, MD, Department of Ophthalmology and Visual Science, Kumamoto University Graduate School of Medical Sciences, 1-1-1 Honjo, Kumamoto, 860-8556, Japan (tanihara@pearl.ocn.ne.jp).
Author Contributions: *Study concept and design:* Tanihara, Inatani, Honjo, Tokushige, Azuma, and Araie. *Acquisition of data:* Tanihara and Tokushige. *Analysis and interpretation of data:* Tanihara, Inatani, Honjo, Tokushige, Azuma, and Araie. *Drafting of the manuscript:* Tanihara and Tokushige. *Critical revision of the manuscript for important intellectual content:* Tanihara. *Administrative, technical, and material support:* Tanihara, Inatani, Honjo, Tokushige, Azuma, and Araie. *Study supervision:* Tanihara, Inatani, Honjo, Azuma, and Araie.
Financial Disclosure: Drs Tanihara and Azuma are contracted with Senju Pharmaceutical Co, Ltd as medical experts.

REFERENCES

1. Gabelt BT, Kaufman PL. Prostaglandin $F_{2\alpha}$ increases uveoscleral outflow in the cynomolgus monkey. *Exp Eye Res.* 1989;49(3):389-402.
2. Oshika T, Araie M, Sugiyama T, Nakajima M, Azuma I. Effect of bunazosin hydrochloride on intraocular pressure and aqueous humor dynamics in normotensive human eyes. *Arch Ophthalmol.* 1991;109(11):1569-1574.
3. Coakes RL, Brubaker RF. The mechanism of timolol in lowering intraocular pressure in the normal eye. *Arch Ophthalmol.* 1978;96(11):2045-2048.
4. Toris CB, Gleason ML, Camras CB, Yablonski ME. Effects of brimonidine on aqueous humor dynamics in human eyes. *Arch Ophthalmol.* 1995;113(12):1514-1517.
5. Lippa EA, Carlson LE, Ehinger B, et al. Dose response and duration of action of dorzolamide, a topical carbonic anhydrase inhibitor. *Arch Ophthalmol.* 1992;110(4):495-499.
6. Gaasterland D, Kupfer C, Ross K. Studies of aqueous humor dynamics in man. IV: effects of pilocarpine upon measurements in young normal volunteers. *Invest Ophthalmol.* 1975;14(11):848-853.
7. Nobes C, Hall A. Regulation and function of the Rho subfamily of small GTPases. *Curr Opin Genet Dev.* 1994;4(1):77-81.
8. Narumiya S. The small GTPase Rho: cellular functions and signal transduction. *J Biochem (Tokyo).* 1996;120(2):215-228.
9. Ishizaki T, Naito M, Fujisawa K, et al. p160ROCK, a Rho-associated coiled-coil forming protein kinase, works downstream of Rho and induces focal adhesions. *FEBS Lett.* 1997;404(2-3):118-124.
10. Nakagawa O, Fujisawa K, Ishizaki T, Saito Y, Nakao K, Narumiya S. ROCK-I and ROCK-II, two isoforms of Rho-associated coiled-coil forming protein serine/threonine kinase in mice. *FEBS Lett.* 1996;392(2):189-193.
11. Honjo M, Tanihara H, Inatani M, et al. Effects of Rho-associated protein kinase inhibitor, Y-27632, on intraocular pressure and outflow facility. *Invest Ophthalmol Vis Sci.* 2001;42(1):137-144.
12. Rao PV, Deng PF, Kumar J, Epstein DL. Modulation of aqueous humor outflow facility by the Rho kinase-specific inhibitor Y-27632. *Invest Ophthalmol Vis Sci.* 2001;42(5):1029-1037.
13. Waki M, Yoshida Y, Oka T, Azuma M. Reduction of intraocular pressure by topical administration of an inhibitor of the Rho-associated protein kinase. *Curr Eye Res.* 2001;22(6):470-474.
14. Tokushige H, Inatani M, Nemoto S, et al. Effects of topical administration of Y-39983, a selective Rho-associated protein kinase inhibitor, on ocular tissues in rabbits and monkeys. *Invest Ophthalmol Vis Sci.* 2007;48(7):3216-3222.
15. Wiederholt M, Thieme H, Stumpff F. The regulation of trabecular meshwork and ciliary muscle contractility. *Prog Retin Eye Res.* 2000;19(3):271-295.
16. Amano M, Ito M, Kimura K, et al. Phosphorylation and activation of myosin by Rho-associated kinase (Rho-kinase). *J Biol Chem.* 1996;271(34):20246-20249.
17. Kimura K, Ito M, Amano M, et al. Regulation of myosin phosphatase by Rho and Rho-associated kinase (Rho-kinase). *Science.* 1996;273(5272):245-248.
18. Kureishi Y, Kobayashi S, Amano M, et al. Rho-associated kinase directly induces smooth muscle contraction through myosin light chain phosphorylation. *J Biol Chem.* 1997;272(19):12257-12260.
19. Tian B, Geiger B, Epstein DL, Kaufman PL. Cytoskeletal involvement in the regulation of aqueous humor outflow. *Invest Ophthalmol Vis Sci.* 2000;41(3):619-623.
20. Koga T, Koga T, Awai M, Tsutsui J, Yue BY, Tanihara H. Rho-associated protein kinase inhibitor, Y-27632, induces alterations in adhesion, contraction and motility in cultured human trabecular meshwork cells. *Exp Eye Res.* 2006;82(3):362-370.
21. Rao PV, Deng P, Sasaki Y, Epstein DL. Regulation of myosin light chain phosphorylation in the trabecular meshwork: role in aqueous humour outflow facility. *Exp Eye Res.* 2005;80(2):197-206.
22. Tokushige H. ROCK inhibitor and glaucoma. *Bio Clinica.* 2002;17(13):1191-1194.
23. Fukiage C, Mizutani K, Kawamoto T, Azuma M, Shearer TR. Involvement of phosphorylation of myosin phosphatase by ROCK in trabecular meshwork and ciliary muscle contraction. *Biochem Biophys Res Commun.* 2001;288(2):296-300.

Proceedings of the 29th Annual International
Conference of the IEEE EMBS
Cité Internationale, Lyon, France
August 23-26, 2007.

Three-Dimensional Reconstruction of Optic Nerve Head from Stereo Fundus Images and Its Quantitative Estimation

Toshiaki Nakagawa, Yoshinori Hayashi, Yuji Hatanaka, Akira Aoyama, Takeshi Hara, Akihiro Fujita, Masakatsu Kakogawa, Hiroshi Fujita, and Tetsuya Yamamoto

Abstract— **It is important for diagnosis of glaucoma to grasp 3-D structure of an optic nerve head (ONH). The quantitative 3-D reconstruction of the ONH is required for the diagnosis. We propose a technique to obtain the depth value from stereo image pair of a retinal fundus for the 3-D reconstruction of the ONH. Our technique mainly consists of four steps: (1) cutout of the ONH region from the fundus images, (2) registration of the stereo pair, (3) disparity detection, and (4) depth calculation. For quantitative estimation of the depth value measured by using this method, the depth value was compared with the measurement results determined from the Heidelberg Retina Tomograph (HRT), which is a confocal laser-scanning microscope. As a result, the depth value of the ONH obtained using the stereo retinal image pair was in accordance with that obtained using the HRT (r=0.91). These results indicate that the stereo fundus images could be useful for assessing the depth value of the ONH for the diagnosis of glaucoma.**

I. Introduction

The cup/disc (C/D) ratio, which is the ratio of the diameter of the depression (cup) to that of the optic nerve head (ONH, disc), is one of the important parameters for an early diagnosis of glaucoma. The C/D ratio is generally used in clinical practice because its value is greater in the case of glaucoma. The interpretation of the ONH, which actually has a 3-D structure, by using a 2-D image is subjective and there is a wide variation between the examination of the ONH by different observers and even between the examinations by the same observer [1]. A more quantitative alternative is to use the Heidelberg Retina Tomograph (HRT), which is a confocal laser-scanning microscope, for the acquisition and analysis of the 3-D measures of the ONH [2, 3]. It has been revealed that an HRT is capable of ONH imaging, and it is an established technique for detecting glaucomatous structural changes.

A computerized technique for the qualitative estimation of the depth of the ONH from the stereoscopic pairs of retinal-fundus images has been suggested for the 3-D analysis of the depression of the ONH [4, 5]. It has been shown that this technique is useful for the investigation of the 3-D measures of the ONH. However, the experimental results regarding the quantitative depth value calculated from the stereo image pair of the ONH have not been reported. Moreover, there have been no studies in which the depth value calculated from the stereo image pair has been compared with the HRT outputs.

In this study, an automatic method for reconstructing the 3-D structure of the ONH by using the stereo fundus images is proposed. In order to evaluate the accuracy of our method, the depth values of the ONH obtained from the stereo fundus image pairs are compared with the HRT measurement results.

Manuscript received April 2, 2007. This work was supported in part by a grant for the "Knowledge Cluster Creation Project" from the Ministry of Education, Culture, Sports, Science and Technology (MEXT), Japan.

T. Nakagawa, Y. Hayashi, A. Aoyama, T. Hara, H. Fujita and T. Yamamoto are with the Graduate School of Medicine, Gifu University, 1-1 Yanagido, Gifu 501-1194, Japan (e-mail: nakagawa@fjt.info.gifu-u.ac.jp).

Y. Hatanaka is with the Department of Electric Control Engineering, Gifu National College of Technology, 2236-2 Kamimakuwa, Motosu, Gifu 501-0495, Japan.

A. Fujita is with the Kowa Company, Ltd., 1-3-1 Shinmiyakoda, Hamamatsu, Shizuoka 431-2103, Japan.

M. Kakogawa is with the TAK Co., Ltd., 4-35-12 Kono, Ogaki, Gifu 503-0803, Japan.

II. Methodology

In our technique, the depth value is obtained from the stereo fundus image pair; it mainly consists of four processes. A stereo image pair consists of a "left image" and a "right image" captured from different perspectives. The stereo image pair can be generated by taking two shots with a parallel shift using a single-lens fundus camera or by taking a single shot using a stereo-fundus camera. In the first step, the images of the ONH region are cut out from the original fundus images in the first step. In the second step, the registration process of the stereo ONH image pair is performed in order to remove any displacements. In the third step, the "corresponding points" in each stereo ONH image are detected. In the fourth step, the depth values of the 3-D structures are calculated from the results of the disparities detected in the configuration of the corresponding points.

A. Cutout of the ONH region

The images of the ONH region were cut out from the original stereo image pair in order to reduce the processing area to expedite the subsequent steps. In this processing step, the fundus images were cropped to form quadrates at the position of the ONH region that was extracted automatically. The ONH region has relatively high pixel values in three channels (R, G, and B components) in the color stereo fundus image pairs. P-tile thresholding [6] can be applied to define a threshold for an approximate extraction of the ONH region because individual variations of the ONH do not vary significantly.

The blood vessels (BVs) running on the surface of the ONH interfered with the correct extraction of the ONH region

1-4244-0788-5/07/$20.00 ©2007 IEEE

in the P-tile thresholding operation. In order to solve this problem, the extraction of the ONH region was performed by using the images in which the BVs were erased. These erased pixels were then interpolated by using the RGB values of the pixels in the surrounding region. The pixel value P used in the interpolation was calculated as

$$P=\frac{\sum_{k=1}^{n}\frac{p_k}{l_k}}{\sum_{k=1}^{n}\frac{1}{l_k}}, \quad (1)$$

where p_k denotes the value of the pixels in the surrounding region, n is the number of surrounding pixels, and l_k is the distance between the interpolated pixel and each surrounding pixel.

The BVs were extracted by using the black-top-hat transformation, which is a type of grayscale morphological operation, from the G-component of the color fundus images. The structure element used in this transformation was a disc whose diameter was set to the same level as the thickness of the BVs in the ONH region. The regions containing BVs were extracted after applying the Otsu thresholding technique [7] to the black-top-hat-transformed image.

The center of the square of the cutout of the ONH region was the gravity point of the ONH region extracted from the images in which the BVs were erased. In this study, the size of the original fundus image was 1600 × 1200 pixels, the angle of view was 27°, and the size of the cutout region was 512 × 512 pixels, as shown in Fig. 1.

B. Registration of the stereo fundus image pair

The disparity, which is defined as the difference in the position of the corresponding points in the stereo image pair, depends on the change in the position of not only the camera but also the subject (subject's motion). The disparity due to the subject's motion affects the calculated result of the depth value. In order to accurately measure the depth value, it is necessary to rectify the disparity due to the subject's motion. However, it is difficult to determine the motion that induces the disparity only on the basis of observations.

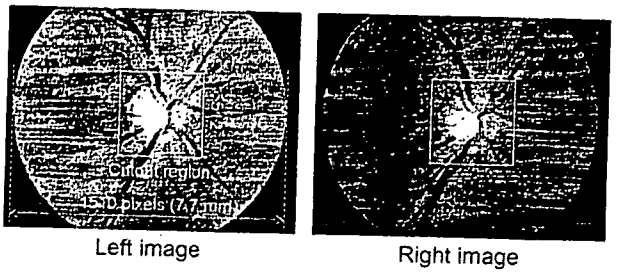

Fig. 1. Example of an original stereo fundus image pair and cutout region from the left and right images.

In the retinal fundus, the bell-shaped ONH has a dent on the opposite side, that is, the side facing the camera. Therefore, the cup region of the ONH exists at a distant position from the camera and the disparity is small. Theoretically, it is possible to use the pixels in the ONH region, which have small disparities, for image registration. However, the region of the retina around the ONH is more suitable for the image registration task because the blood vessels in the retina exist even on the curved surface; in this region, the right and left images exhibit a parallel shift. Moreover, the 3-D structure of the retinal region is simpler than that of the ONH. From the abovementioned description, the image registration for rectifying the disparity due to a subject's motion was performed by using the pixels from regions other than the ONH region.

In order to exclude the ONH region from the registration process, the pixels of a fundus image were allocated to two regions: the retina and the ONH region. The pixels in the retina region were used for registering the stereo image pair. The boundary between the two regions was obtained by automatically extracting the ONH region.

In the first step, a contour of the ONH region was extracted from two stereo fundus images. The ONH region has a tendency to have a higher pixel value than the other regions. Furthermore, the contour of the ONH region can be expressed with a smooth closed curve in many cases. Therefore, the contour that exhibits high edge intensity, which is defined as a change in the brightness, was extracted as the smooth closed curve by using an active-contour model [8].

In the next step, the registration of the stereo image pair was performed by using all the pixels of the images from regions other than the ONH region. If the positional error is minimum, the sum of all the differences between the pixel values of the two images will be minimum. Therefore, the right image was translated and rotated until the sum of all the differences was minimum. This registration procedure used the cross-correlation r between the two images, which is calculated as

$$r=\frac{\sum_{i=0}^{W}\sum_{j=0}^{H}\{L(i,j)-\bar{L}\}\{R(i,j)-\bar{R}\}}{\sqrt{\sum_{i=0}^{W}\sum_{j=0}^{H}\{L(i,y)-\bar{L}\}^2}\sqrt{\sum_{i=0}^{W}\sum_{j=0}^{H}\{R(i,j)-\bar{R}\}^2}}, \quad (2)$$

where L and R are the feature values in the coordinate system (i, j) of the left and right images, respectively; W and H, the width and height of the image, respectively; and $\bar{L}$ and $\bar{R}$, the average pixel values in the left and right images, respectively. The features used in the registration were the pixel values of the RGB components and its edge images created by the Sobel filter using the RGB values.

C. Disparity detection

The required disparity for obtaining the depth value was calculated from the location differences between the corresponding points. The detection of the corresponding points was performed using the pixels of the area within the registered ONH image pair. The detection of the corresponding points comprised the search for a point on the right image that corresponded to the reference point on the left image. The search was performed by setting up regions of interest (ROIs) including the pixels around the reference point and the candidate point separately. Two points on the left and right images having a similar texture in their respective ROIs were regarded as the corresponding points. The similarity was measured by the cross-correlation r defined as

$$r = \frac{\sum_{i=-W/2}^{W/2}\sum_{j=-H/2}^{H/2}\{L(x_L+i,y_L+j)-\bar{L}\}\{R(x_R+i,y_R+j)-\bar{R}\}}{\sqrt{\sum_{i=-W/2}^{W/2}\sum_{j=-H/2}^{H/2}\{L(x_L+i,y_L+j)-\bar{L}\}^2}\sqrt{\sum_{i=-W/2}^{W/2}\sum_{j=-H/2}^{H/2}\{R(x_R+i,y_R+j)-\bar{R}\}^2}}, \quad (3)$$

where L and R are the feature values of the pixels in the ROIs set in the ONH image pair, $\bar{L}$ and $\bar{R}$ are the average feature values of the ROIs, (x_L, y_L) is the coordinate of the reference point in the left image, (x_R, y_R) is the coordinate of the candidate point in the right image, and W and H are the width and height of the ROI, respectively.

The features used in the detection of the corresponding points were the pixel values of the RGB components and its edge images created by the Sobel filter using the RGB value. The parameters of this process are shown in Fig. 2. The size of the ROI was set to 21 × 21 pixels and the searching range was set to 41 × 23 pixels ([x_L – 5 pixels, x_L + 15 pixels]). The reference points arranged in the equally spaced positions and the interval were set to 4 pixels. The point having the maximum cross-correlation coefficient was considered to be the corresponding point. When the maximum value of the cross-correlation coefficient was smaller than a preset threshold value, it was assumed that the corresponding point of the reference point was not found. The disparity of the point that did not have a corresponding point was interpolated by the average of the disparities of the surrounding reference points.

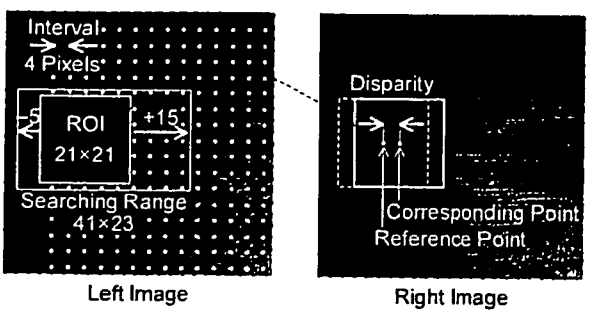

Fig. 2. Parameters in detecting the corresponding points in the left and right images.

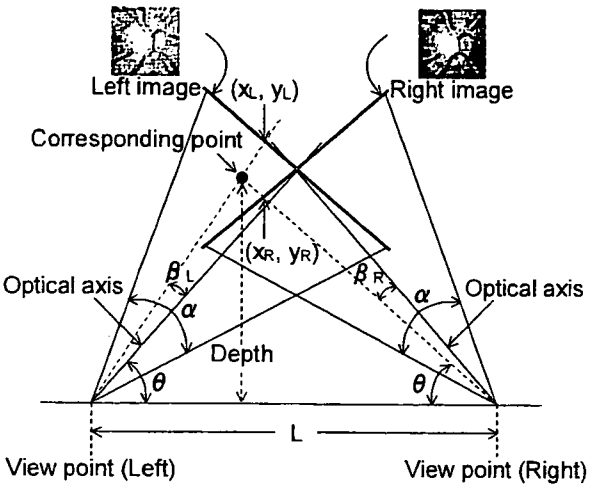

Fig. 3. Convergent visual system for depth calculation of stereo image pair.

D. Depth calculation

The depth value of the 3-D position was determined according to the value of the disparity in each location of the reference point. The depth value was calculated as

$$Depth = \frac{L \times \tan(\theta-\beta_L)\times\tan(\theta+\beta_R)}{\tan(\theta-\beta_L)+\tan(\theta+\beta_R)}, \quad (4)$$

$$\beta_L = \tan^{-1}\{x_L \times \tan(\frac{\alpha}{2}\times\frac{\pi}{180})\times\frac{2}{W}\}, \quad (5)$$

$$\beta_R = \tan^{-1}\{x_R \times \tan(\frac{\alpha}{2}\times\frac{\pi}{180})\times\frac{2}{W}\}, \quad (6)$$

and

$$x_R = x_L + disparity, \quad (7)$$

where x_L and x_R are the horizontal coordinates of the corresponding points in the left and right images, respectively. The original points in the coordinate system were arranged on the optical axis of the left and right viewpoints. α is the angle of view of the images; β, the angle between the position of the corresponding point and the optical axis; W, the width of the images; and L, the length of the baseline, which is the distance between the optical centers of the camera.

III. Results and Discussions

The proposed technique was evaluated using 12 normal fundus stereo image pairs. Figure 4 shows the depth values of the same ONH measured using the stereo image pairs and the HRT. The results of the depth measurements using the stereo image pairs agreed well with the results of the HRT at

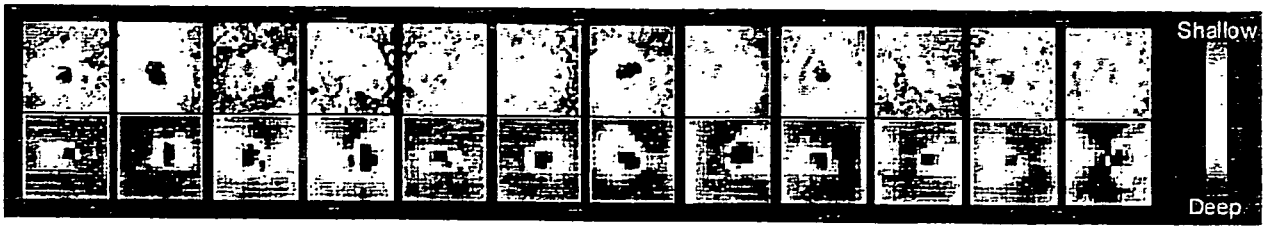

Fig. 4. The upper row shows the depth maps of the OHN from stereo fundus image pairs. The lower row shows the depth maps obtained using the HRT. The depth of the ONH obtained using the stereo images agreed with the results obtained using the HRT.

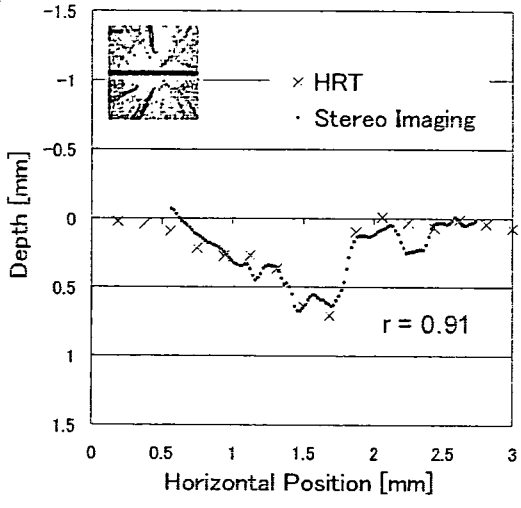

Fig. 5. Example of depth information obtained from the stereo fundus image pair and HRT.

corresponding levels. The depth values measured using the stereo image pairs fluctuated. This is due to the slight uncertainty in the disparity detection. It is presumed that the median filter can effectively eliminate this incorrect disparity. Figure 5 shows the profile trace along the center of the OHN. The correlation coefficient r between the two results obtained by the two methods was 0.91. This result indicates the validity of proposed method to obtain quantitative depth values.

IV. Conclusion

In this study, we conducted quantitative measurements of the depth value of an ONH region from the stereo fundus images. The depth values obtained from the stereo image pairs were in accordance with the results of the HRT. These depth values may be useful as assisting parameters for ophthalmologists in the diagnosis of the degree of glaucoma.

Acknowledgment

This work was partly supported by a grant for the Knowledge Cluster Creation Project from the Ministry of Education, Culture, Sports, Science and Technology, Japan. The authors would like to acknowledge the contribution of Dr. R. Shiraki of the Shiraki Eye Clinic for the acquisition of the HRT data.

References

[1] J. M. Tielsch, J. Katz, H. A. Quigley, A. Sommer, "Intraobserver and interobserver agreement in measurement of optic disc characteristics," Opthalmol., vol.95, no.3, pp.350–356, 1988.

[2] F. S. Mikelberg, C. M. Parfitt, N. V. Swindale, S. L. Graham, S. M. Drance, R. Gosine, "Ability of the Heidelberg Retina Tomograph to detect early glaucomatous visual field loss," J. Glaucoma, vol.4, no.4, pp.242–247, 1995.

[3] M. Iester, F. S. Mikelberg, S. M. Drance, "The effect of optic disc size on diagnostic precision with the Heidelberg Retina Tomograph," Ophthalmol., vol.104, no.3, pp.545–548, 1997.

[4] E. Corona, S. Mitra, M. Wilson, T. Krile, Y. H. Kwon, P. Soliz, "Digital stereo image analyzer for generating automated 3-D measures of optic disc deformatin in glaucoma, IEEE Trans. Med. Imaging, vol.21, no.10, pp.1244–1253, 2002.

[5] J. Xu, O. Chutatape, "Auto-adjusted 3-D optic disk viewing from low-resolution stereo fundus image," Computers in Biology and Medicine, vol.36, pp.921–940, 2006.

[6] J. R. Parker, "Algorithms for Image Processing and Computer Vision," Wiley Computer Publishing, 1997.

[7] N. Otsu, "A threshold selection method from gray-level histograms," IEEE Trans. Syst. Man. Cybern. vol.SMC-9, pp.62–66, 1979.

[8] M. Kass, A. Witikin, D. Terzopoulos, "Snakes: Active contour models," Int. J. Computer Vision, vol.1, pp.321–331, 1987.

Jpn J Ophthalmol 2007;51:379–389

DOI 10.1007/s10384-007-0468-8

CLINICAL INVESTIGATION

Decreased Nasal–Temporal Asymmetry of the Second-Order Kernel Response of Multifocal Electroretinograms in Eyes with Normal-Tension Glaucoma

Eijiro Asano[1], Kiyofumi Mochizuki[1], Akira Sawada[1], Ei-ichiro Nagasaka[2], Yuji Kondo[1], and Tetsuya Yamamoto[1]

[1]Department of Ophthalmology, Gifu University Graduate School of Medicine, Gifu, Japan; [2]Mayo Corporation, Inazawa, Japan

Abstract

Purpose: To determine whether multifocal electroretinograms (mfERGs) can provide an index for identification of glaucomatous optic neuropathy in patients with normal-tension glaucoma (NTG).

Methods: mfERGs were recorded in 30 normal volunteers (30 eyes) and 20 patients (20 eyes) with normal-tension glaucoma (NTG). Visual field examinations were performed with a Humphrey field analyzer, and all NTG patients had unilateral hemifield defects. The mfERGs were elicited by a binary m-sequence of flashes from 37 hexagonal elements that subtended an overall visual angle of 50° × 40°. The mfERGs were summed and analyzed for predetermined retinal loci. These mfERGs were compared with the perimetric findings of the corresponding visual fields.

Results: In normal volunteers, the amplitude of the second-order kernel within the central 5° of the nasal hemisphere was significantly smaller than in that of the temporal hemisphere (Wilcoxon signed-rank test, $P = 0.0001$). In NTG patients, this asymmetry of the two hemispheres was reduced or not present. The ratio of the amplitude of the mfERGs from the nasal and temporal hemispheres (N/T amplitude ratio) in normal control volunteers was significantly different from that of NTG patients with a hemifield defect (analysis of variance, $P = 0.0001$). When the cutoff value for the N/T amplitude ratio was set at 0.83 for discriminating glaucomatous eyes from normal eyes, the sensitivity was 65.0% with a specificity of 96.7%. The area under the receiver–operating characteristic curve of the N/T amplitude ratio was 0.86. The N/T amplitude ratio and the visual field indices were significantly correlated.

Conclusion: A decrease in the nasal–temporal asymmetry in the amplitude of the second-order kernel responses within the central 5° of glaucoma patients' eyes indicated a dysfunction of the inner retinal layers, including of the retinal ganglion cells. **Jpn J Ophthalmol** 2007;51:379–389 © Japanese Ophthalmological Society 2007

Key Words: hemifield visual field defects, multifocal electroretinogram, normal-tension glaucoma

Introduction

A number of electrophysiological tests have been used to determine whether the alterations of retinal function in glaucomatous eyes can be detected objectively. The main site of damage in eyes with glaucoma is most likely the lamina cribrosa,[1] and the damage eventually spreads retrogradely to the cell bodies of the retinal ganglion cells (RGCs). The dysfunction in glaucomatous eyes is in the RGCs and their axons. Therefore, standard flash electroretinograms (ERGs) do not provide critical information on early glaucomatous changes, because the cells generating conventional ERGs are located in the outer retina.[2] Thus, the functioning of the retina distal to the RGCs in glaucomatous optic neuropathy has been considered normal.[3,4]

Received: February 22, 2007 / Accepted: June 7, 2007
Correspondence and reprint requests to: Kiyofumi Mochizuki, Department of Ophthalmology, Gifu University Graduate School of Medicine, 1-1 Yanagido, Gifu-shi 501-1194, Japan
e-mail: mochi-gif@umin.ac.jp

Jpn J Ophthalmol
Vol 51: 379–389, 2007

The techniques for recording multifocal electroretinograms (mfERGs) have been refined, and the search for an objective method to detect the pathological changes in glaucomatous eyes has continued with mfERGs. Thus, Bearse et al.[5] suggested that the second-order kernels of mfERGs might have a component that indicates a decrease in surviving RGCs throughout the retina in glaucomatous eyes. Sutter and Bearse[6,7] extracted an optic nerve head component (ONHC) from the second-order kernel of mfERGs, and suggested that this ONHC was a signal originating from RGCs and was altered in eyes with glaucomatous optic neuropathy. In addition, they reported that the spatial distribution of the amplitudes of the ONHC in normal subjects was steeper than that of the other retinal components, with a peak in the center of the visual field.[6] From these findings, we assumed that the mfERGs elicited from the central retina receive a larger contribution from the ONHC than more peripheral mfERGs.

Studies on glaucomatous eyes using mfERGs have been performed with flicker stimulation,[8–10] global flash stimuli,[11] s-wave stimulation,[12] and low-contrast stimuli.[8,13,14] In these studies, no significant differences were found in the amplitudes of mfERGs between glaucoma and control subjects,[9] and only a slight prolongation of latencies was found in eyes with glaucoma.[8,10,11] Moreover, they found no significant correlation between the amplitudes of the mfERGs and visual field parameters. One of the reasons for the lack of differences might be that the slight alterations of the ONHC were buried in the larger retinal components when the responses were grouped in relatively large quadrants or rings over the entire stimulus field.

Several studies on normal eyes have shown that the amplitudes of mfERGs in the nasal hemifield are significantly different from those in the temporal hemifield, that is, there is a nasal–temporal (N/T) asymmetry.[5,6,13–16] We hypothesized that this asymmetry was related to local differences in the distribution of the ONHC, and, thus, this asymmetry should be altered by dysfunction of the RGCs in glaucomatous eyes. Our analyses focused on the changes of mfERGs around the central region, because we believe that the small difference in the ONHC between normal and glaucomatous eyes should be detected more clearly in this region. We also analyzed the ratio of the amplitudes of the mfERGs from the nasal and temporal hemispheres and between the superior and inferior hemispheres to search for any alterations in asymmetry in the mfERGs.

Subjects and Methods

Control and Normal-Tension Glaucoma Subjects

Data were obtained from 30 control volunteers (30 eyes) and 20 patients (20 eyes) with normal-tension glaucoma (NTG). The criteria used to select the control subjects were normal findings on all ocular examinations, best-corrected visual acuity of 20/30 or better, normal visual fields, and no history of ocular or neurological diseases.

Although glaucoma is characterized by a unique pattern of visual field defects that correspond to the optic nerve head excavation, the extent of glaucomatous visual field defects is highly variable among patients. We selected NTG patients with visual field defects confined to one hemifield, because mfERG abnormalities would be more easily detected in the summed mfERGs in this type of patient. Patients were diagnosed with NTG when they were found to have the following: visual field loss distinctive to glaucoma, cupping of the optic nerve head, and intraocular pressure of <20 mmHg, including 24-h diurnal values. In addition, all of the NTG patients had visual field abnormalities of 5 dB or greater at two or more adjacent points, or abnormalities of 10 dB or greater at one or more points, below the age-adjusted average control value according to a Statpac single-field analysis. Although the glaucoma subjects could have some normal findings during ocular examinations, they all had glaucomatous optic neuropathy, no history of any medications that could affect pupil diameter, no history of any ocular surgery, and a best-corrected visual acuity of 20/30 or better.

Written informed consent was obtained from all participants, and all procedures were performed in compliance with the tenets of the Declaration of Helsinki. The experimental protocols were approved by the Institutional Board of Research Associates of Gifu University Graduate School of Medicine.

Visual Field Testing

All visual field examinations were performed with a Humphrey field analyzer (Zeiss-Humphrey, San Leandro, CA, USA) using the central 30-2 static threshold program. Results that met the reliability criteria for false-negative responses of <30%, false-positive responses of <15%, and fixation loss rates of <15% were used for the analyses.

The glaucoma patients were divided into two groups according to their visual field defects; those with defects in the superior hemifield were placed in one group, and those with defects in the inferior hemifield in a second group. The presence of a unilateral hemifield defect was defined on the basis of the total deviation probability plot as a hemifield with eight or more test points with $P < 5\%$, either in a cluster or sporadically dispersed. In contrast, an intact hemifield was defined as one with no points worse than the 2% probability level, and no more than two points at the 2%–5% probability level.[17]

Multifocal ERG Techniques

A Visual Evoked Response Imaging System Science 4 (Electro-Diagnostic Imaging, EDI, Redwood City, CA, USA) was used to record the mfERGs. The eye used for the recordings was optically corrected, and the pupil was dilated to at least 8 mm in diameter with topical 0.5% tropicamide and 0.5% phenylephrine (Mydrin-P; Santen Phar-

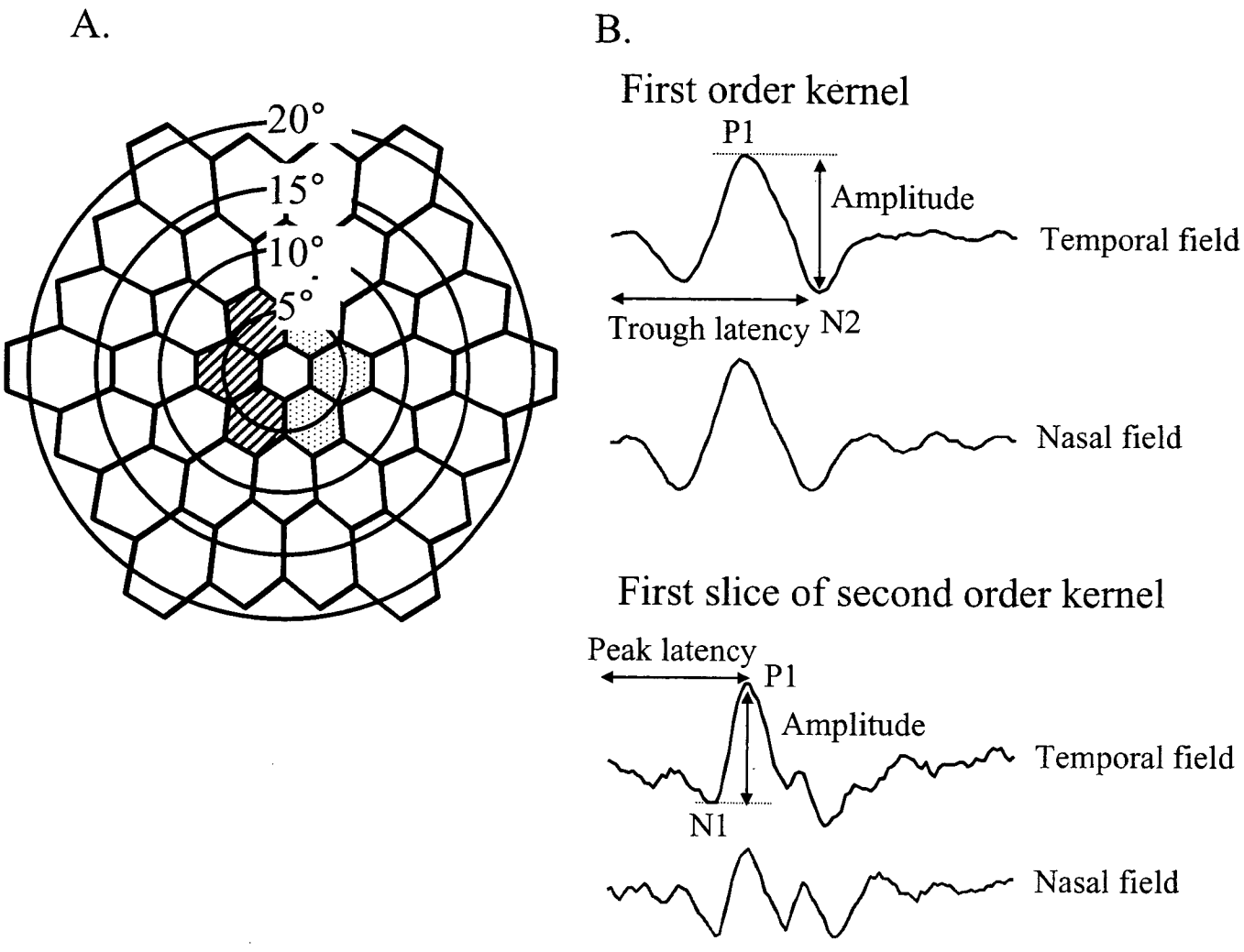

Figure 1A, B. Pattern of the 37-hexagon stimulus array with circles indicating radii of 5°, 10°, 15°, and 20°. **A** Waveforms and measurements of the first-order kernel response (*upper right*), and the first slice of the second-order kernel response (*lower right*) obtained from multifocal electroretinograms (**B**).

maceutical, Osaka, Japan). A bipolar contact lens electrode (Mayo, Inazawa, Japan) was placed on the cornea, which was anesthetized with topical oxybuprocaine hydrochloride (Benoxil). The contralateral eye was covered. Hydroxyethylcellulose gel (Scopisol) was used to keep the cornea moist and to form a good electrical contact between the contact lens electrodes and the cornea. A gold-cup electrode was attached to the right earlobe and served as the ground.

The visual stimulus consisted of 37 hexagons that were displayed on a monochrome computer monitor (QB1781; Chuomusen, Tokyo, Japan). The overall area subtended by the stimulus pattern was 50° by 40° (Fig. 1A). Each element was independently alternated between black (5 cd/m^2) and white (200 cd/m^2) at a frame rate of 75 Hz according to a binary m-sequence. The contrast of the hexagons was 95.1%. The mfERGs were recorded with bandpass filters of 10 to 300 Hz, and the total recording time was approximately 8 min. Recordings with eye movements or blinks causing artifacts were discarded and recorded again. An artifact elimination technique was applied once; however, spatial smoothing was not used.

Response Analyses

The first negative trough (N1), the first positive peak (P1), and the second negative trough (N2) were studied. The amplitude from P1 to N2 of the first-order kernel response, and that from N1 to P1 of the first slice of the second-order kernel response, were used in the analyses. In addition, the latencies of N2 of the first-order kernel and P1 of the second-order kernel (Fig. 1B) were measured.

For the analyses, the mfERGs were initially grouped into three concentric rings; central, middle, and peripheral rings (Figs. 2A and B). Then, the mfERGs from the superior field in each ring were summed and compared with the summed mfERGs in the inferior ring. Similarly, the summed mfERGs from each ring in the nasal hemisphere were compared with

Jpn J Ophthalmol
Vol 51: 379–389, 2007

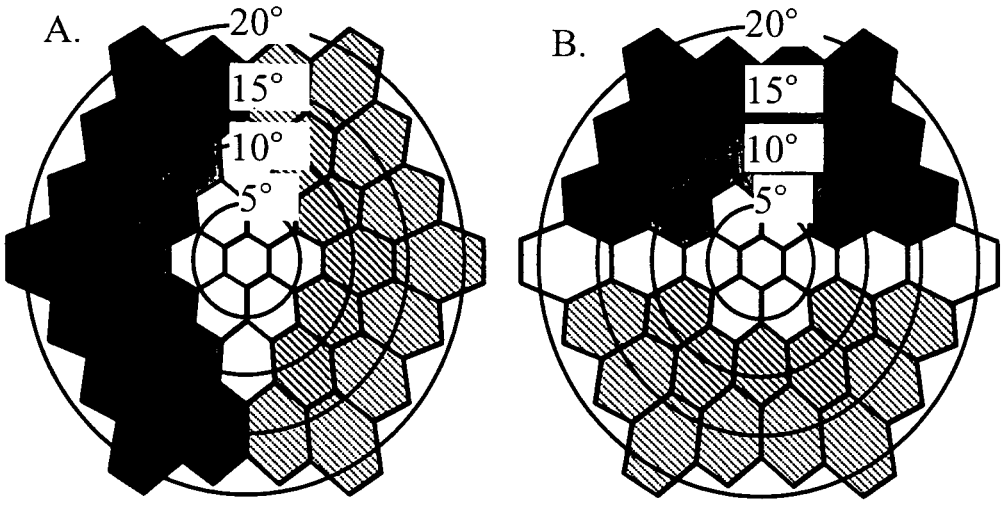

Figure 2A, B. Pattern of hexagons grouped in concentric rings with similar eccentricities (marked by different shadings). For further analysis, hexagons were separated and averaged according to hemisphere: temporal and nasal hemispheres (**A**), or superior and inferior hemispheres (**B**). Hexagons lying on the horizontal or vertical midline through the macula were not used in the analysis.

Table 1. Demographic data of normal volunteers and NTG patients

	Normal volunteers (30 eyes of 30 subjects)	NTG patients (20 eyes of 20 subjects)	*P* value*
Sex (male/female)	10/20	11/9	0.1283
Right/left	15/15	8/12	0.3541
Age (years)	57.6 ± 10.0 (43–75)	59.7 ± 8.9 (40–73)	0.4399
Refractive error (D)	−0.33 ± 2.10 (−4.75 to +2.75)	−2.51 ± 2.94 (−8.75 to +2.25)	0.0084

Values are means ± SD (range).
NTG, normal-tension glaucoma.
*Mann-Whitney *U* test or Fisher's direct probability test.

the corresponding averaged mfERGs in the temporal hemisphere.

The ratios of the amplitudes of the mfERGs of the nasal to the temporal hemisphere (N/T), and of the superior to the inferior hemisphere (S/I) were calculated to evaluate the asymmetry. For all eyes, the amplitudes, implicit times, and N/T amplitude ratios of the summed responses in the nasal hemifield were compared with the responses in the temporal hemifield. Similarly, the summed responses in the superior hemifield were compared with the summed responses in the inferior hemifield.

To compare the mfERGs with the thresholds measured by Humphrey perimetry of the corresponding visual field, the thresholds in NTG subjects were separately averaged according to distance from the macula, that is, within the central 5°, 10°, 20°, and 30°. We examined the relationships between point thresholds or total deviation obtained from the corresponding visual field area and the N/T amplitude ratio of the first-order kernel response within the central 5°, and of the second-order kernel response within the central 5°.

Statistical Analyses

The Wilcoxon signed-rank test, Mann-Whitney *U* test, and Fisher's direct probability test were used. In addition, one-way analysis of variance (ANOVA) and Scheffé post hoc comparisons were used to determine the statistical significance of the differences in the amplitudes and implicit times in the first- and second-order kernels of the mfERGs among the three groups. Spearman rank correlations were used to assess relationships between point thresholds or total deviation and the N/T amplitude ratio of the first-order kernel and that of the second-order kernel. A *P* value of <0.05 was considered significant.

Results

The demographic data of the control subjects and NTG patients are presented in Tables 1 and 2. The mean age of the normal volunteers was 57.6 ± 10 years (range, 43–75 years), and that of NTG patients was 59.7 ± 8.9 years (range, 40–73 years). The mean refractive error of the NTG patients (−2.51 D) was significantly higher than that of the normal volunteers (−0.33 D; $P = 0.0084$). Of the 20 NTG patients, ten had visual field defects predominantly in the superior hemifield, and ten in the inferior hemifield.

Comparison of First-Order and Second-Order Kernels between Controls and NTG Patients

Representative waveforms of the first-order and second-order kernels of the mfERGs recorded from a normal vol-

Table 2. Demographic data for NTG patients with hemifield visual field defects

	Superior hemifield defect-dominant group (10 eyes of 10 patients)	Inferior hemifield defect-dominant group (10 eyes of 10 patients)	*P* value*
Sex (male/female)	5/5	6/4	>0.9999
Right/left	3/7	5/5	0.6499
Age (years)	61.9 ± 5.20 (60–68)	57.4 ± 11.75 (40–73)	0.6766
Refractive error (D)	−1.28 ± 2.91 (−8.75 to +0.50)	−3.75 ± 2.71 (−6.25 to +2.25)	0.0343
HFA central 30-2			
MD (dB)	−6.67 ± 2.99 (−12.62 to −3.55)	−7.97 ± 4.78 (−15.43 to −1.33)	0.5453
PSD (dB)	12.26 ± 1.66 (9.35–13.84)	11.73 ± 4.30 (6.40–18.36)	0.5453
CPSD (dB)	11.93 ± 1.63 (9.21–13.62)	11.49 ± 4.27 (6.22–18.30)	0.6500

Values are means ± SD (range).
HFA, Humphrey field analyzer; MD, mean deviation; PSD, pattern standard deviation; CPSD, corrected pattern standard deviation.
*Mann-Whitney *U* test or Fisher's direct probability test.

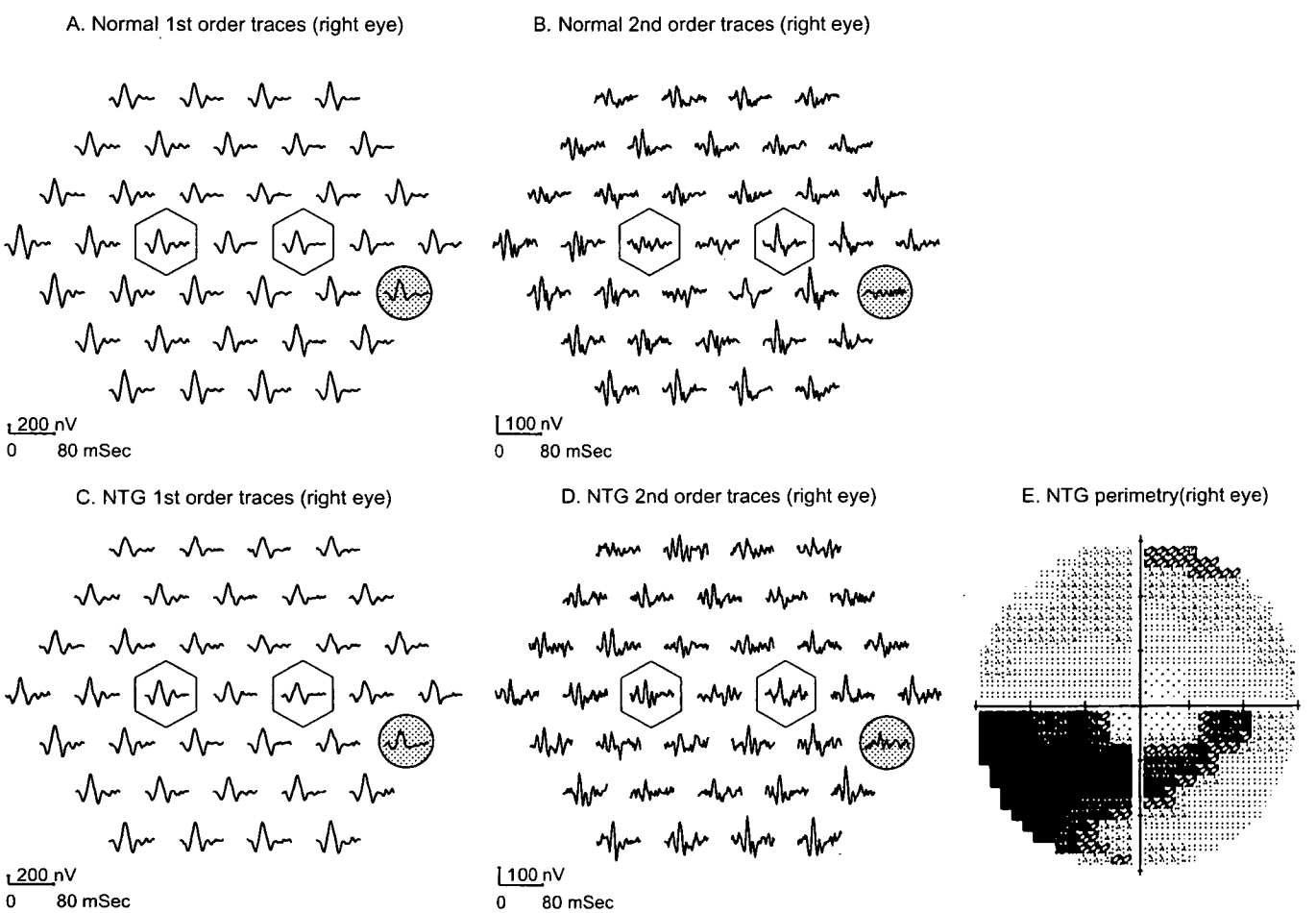

Figure 3. Representative waveforms of the first-order kernel and the first slice of the second-order kernel obtained from a normal volunteer (*upper*) and a normal-tension glaucoma (*NTG*) patient (*lower*).

unteer and a NTG patient are shown in Fig. 3. The amplitude of the second-order kernel for the nasal 5° central hexagon in the normal volunteers was significantly smaller than that of the temporal hemisphere (Fig. 3B, open hexagons). This asymmetry was less or was not present in the NTG patients (Fig. 3D).

Summed Responses from Concentric Rings in Normal Volunteers

In normal volunteers, the amplitudes of the first-order kernel in the temporal and superior hemisphere of all three rings were significantly smaller than those in the corre-

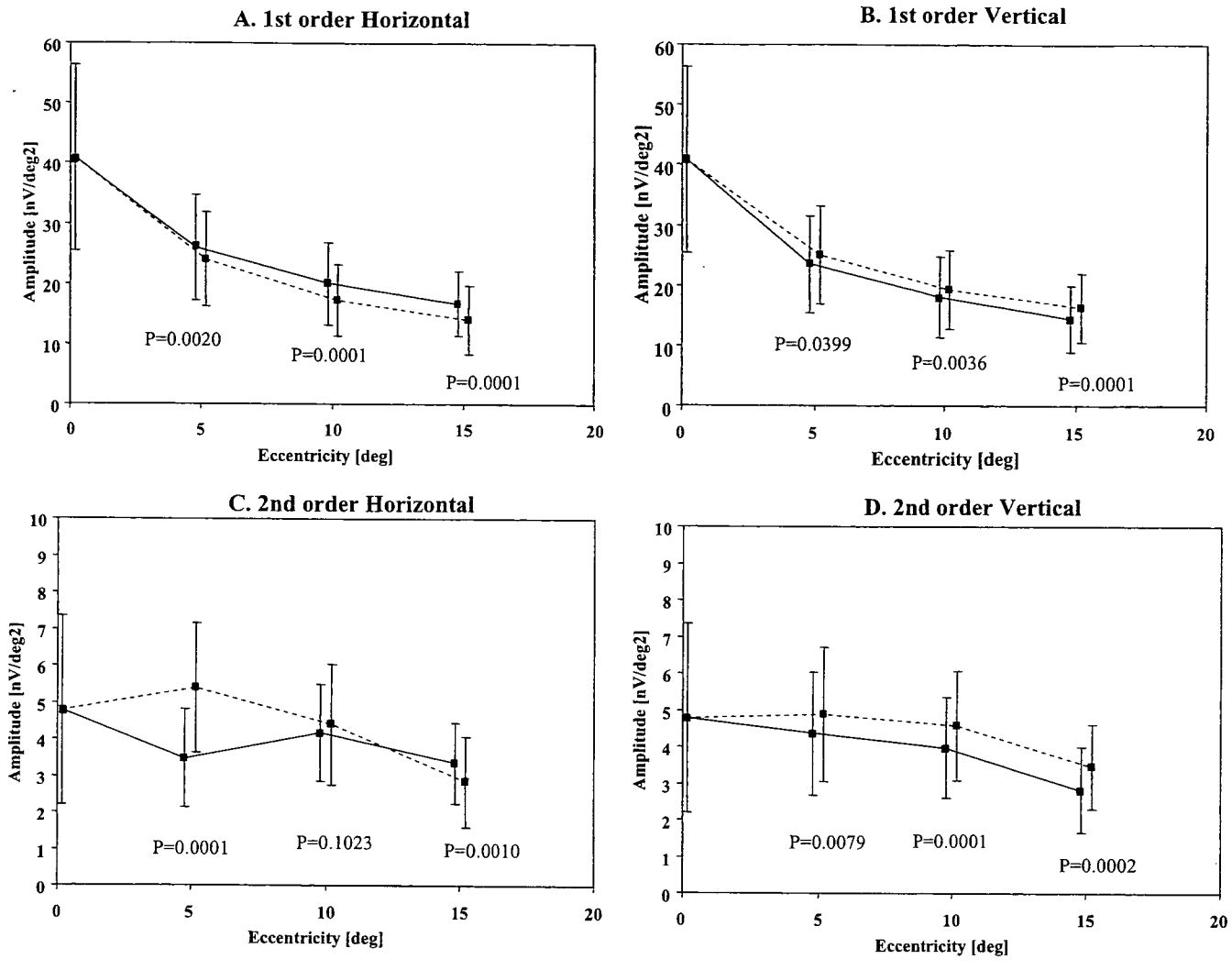

Figure 4A–D. Mean amplitudes of the first-order kernel horizontally from the center to the temporal or nasal retinal region (**A**), and along a vertical line from the center to the superior or inferior retinal region (**B**) in the normal control group. Mean amplitudes of the second-order kernel horizontally from the center to the temporal or nasal retinal region (**C**), and along a vertical line from the center to the superior or inferior retinal region (**D**) in the normal control group. **A, C** *Solid lines*, nasal field; *broken lines*, temporal field. **B, D** *Solid lines*, superior field; *broken lines*, inferior field.

sponding nasal and inferior hemispheres, respectively (Fig. 4; Table 3). The trough latencies of the mfERGs in the temporal hemisphere of all three rings were significantly longer than the corresponding nasal ones (Fig. 5; Table 3). In addition, the trough latency in the superior hemisphere within the central 5° was significantly longer than that of the responses in the inferior hemisphere (Fig. 5; Table 3).

The amplitude of the second-order kernel of the mfERGs in the superior hemisphere was significantly smaller than that in the inferior hemisphere (Fig. 4; Table 4). However, unlike with the first-order kernel, the amplitude of the mfERGs in the central 5° and 10°, but not that of the central 15°, in the nasal hemisphere were smaller than those in the temporal hemisphere ($P = 0.0001$ and 0.1023, respectively, Wilcoxon signed-rank test; Table 4).

The peak latencies of the responses from the superior and inferior hemifields and between the nasal and temporal hemifields in the central 5° were significantly different for the three different rings (Fig. 5; Table 4).

Summed Responses from Concentric Rings in NTG Patients

In general, the pattern of the first-order kernels in NTG patients was similar to that of normal subjects. For all three eccentricities, the amplitudes of the first-order kernel in the temporal and superior hemisphere were smaller than those in the nasal and inferior hemispheres (Table 3). The trough latency in the temporal hemisphere was more prolonged than that in the nasal hemisphere (Table 3). However, there was a difference in the trough latency for the central 10° and 15° between the superior and inferior hemispheres in the superior hemifield-dominant glaucoma group.

Table 3. Parameters of the mfERG first-order kernel response within the central 5° in glaucoma patients compared with that in normal volunteers

	Normal	Superior-dominant	Inferior-dominant	*P* value*			ANOVA *P* value
				Normal	Superior	Inferior	
Amplitude [nV/deg2]							
Nasal hemifield	26.1 ± 8.74	24.6 ± 8.85	22.6 ± 6.52	0.0020	0.0770	0.0069	0.5326
Temporal hemifield	24.1 ± 7.91	22.2 ± 7.66	20.2 ± 6.45				0.3695
Superior hemifield	23.5 ± 8.08	21.2 ± 6.63	19.3 ± 5.25	0.0399	0.1141	0.0068	0.2776
Inferior hemifield	25.0 ± 8.17	23.9 ± 9.82	21.6 ± 6.78				0.5465
Nasal/temporal hemifield	1.08 ± 0.11	1.11 ± 0.09	1.13 ± 0.11				0.4856
Superior/inferior hemifield	0.95 ± 0.13	0.92 ± 0.12	0.91 ± 0.07				0.6127
Trough latency [ms]							
Nasal hemifield	42.5 ± 1.31	42.8 ± 1.60	42.6 ± 1.27	0.0133	0.2864	0.0642	0.8429
Temporal hemifield	42.9 ± 1.30	43.1 ± 1.33	43.1 ± 1.10				0.8695
Superior hemifield	42.5 ± 1.31	43.1 ± 1.75	42.6 ± 1.29	0.0028	0.5750	0.6741	0.5835
Inferior hemifield	43.1 ± 1.31	43.3 ± 1.11	42.9 ± 0.92				0.7457

Values are expressed as mean ± SD.
mfERG, multifocal electroretinogram; ANOVA, analysis of variance.
*Wilcoxon signed-rank test: nasal versus temporal hemifield or superior versus inferior.

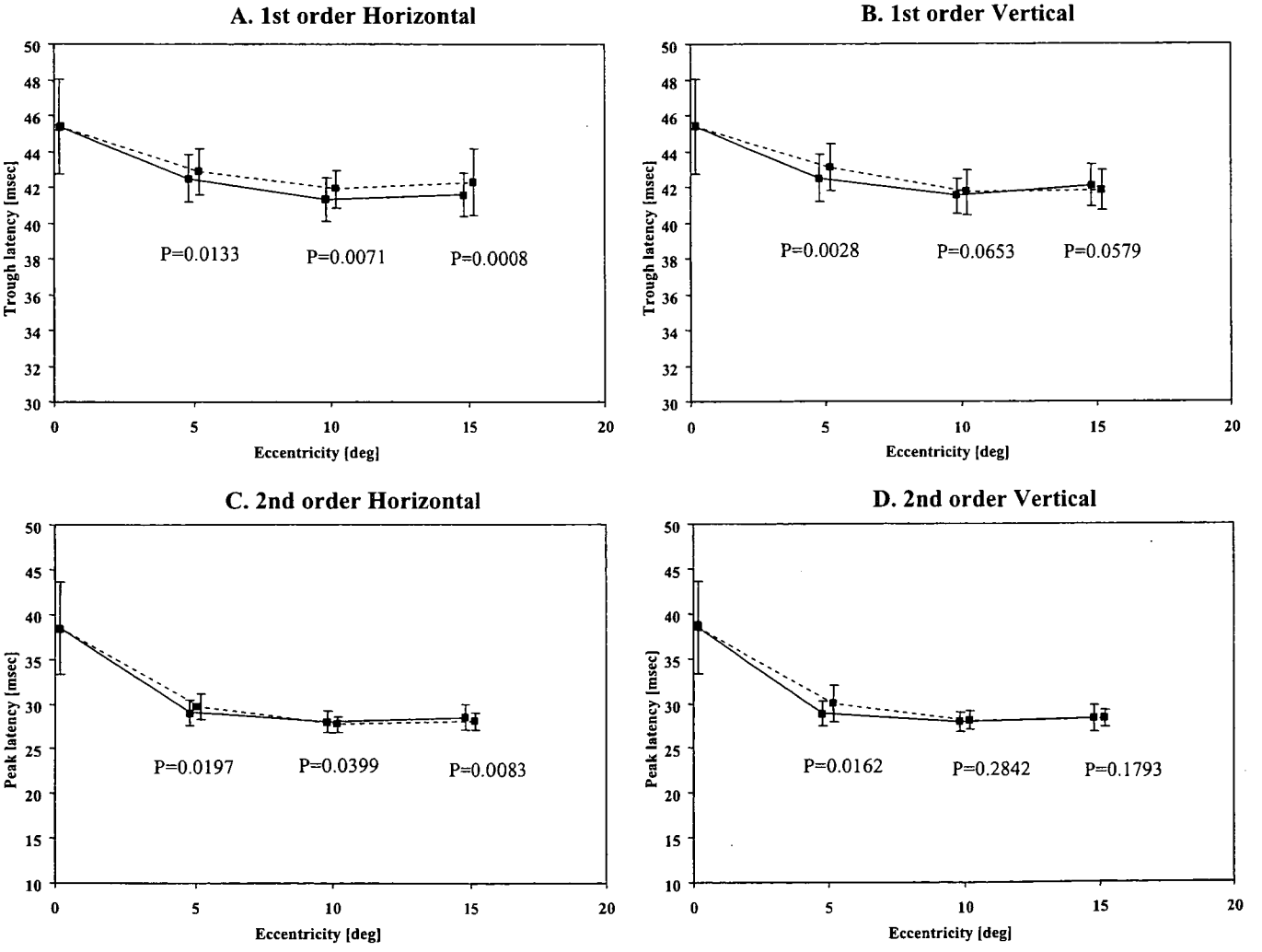

Figure 5A–D. Mean trough latency of the first-order kernel horizontally from the center to the temporal or nasal retinal region (**A**), and vertically from the center to the superior or inferior retinal region (**B**) in the normal control group. Mean peak latency of the second-order kernel response horizontally from the center to the temporal or nasal retinal region (**C**), and vertically from the center to the superior or inferior retinal region (**D**) in normal control groups. **A, C** *Solid lines*, nasal field; *broken lines*, temporal field. **B, D** *Solid lines*, superior field; *broken lines*, inferior field.

Jpn J Ophthalmol
Vol 51: 379–389, 2007

Table 4. Parameters of the MfERG second-order kernel response within the central 5° in glaucoma patients compared with that in normal volunteers

	Normal	Superior-dominant	Inferior-dominant	*P* value*			ANOVA *P* value
				Normal	Superior	Inferior	
Amplitude [nV/deg2]							
Nasal hemifield	3.47 ± 1.33	4.62 ± 2.15	4.38 ± 1.85	0.0001	0.1727	0.1533	0.1094
Temporal hemifield	5.39 ± 1.76	5.16 ± 2.32	5.06 ± 2.01				0.8813
Superior hemifield	4.36 ± 1.69	4.18 ± 1.79	4.14 ± 1.80	0.0079	0.5143	0.6411	0.9229
Inferior hemifield	4.89 ± 1.83	4.35 ± 1.37	4.39 ± 1.58				0.5841
Nasal/temporal hemifield	0.64 ± 0.14	0.91 ± 0.14	0.89 ± 0.21				0.0001
Superior/inferior hemifield	0.90 ± 0.21	0.95 ± 0.22	0.95 ± 0.26				0.7718
Peak latency [ms]							
Nasal hemifield	29.1 ± 1.43	29.1 ± 1.25	29.6 ± 1.01	0.0197	0.4184	0.1573	0.5549
Temporal hemifield	29.7 ± 1.39	29.3 ± 1.11	29.9 ± 1.17				0.6507
Superior hemifield	28.9 ± 1.37	28.9 ± 1.38	29.2 ± 1.25				0.6804
Inferior hemifield	29.9 ± 2.01	29.4 ± 1.11	29.7 ± 1.12	0.0162	0.2008	0.0705	0.7403

Values are expressed as mean ± SD.
*Wilcoxon signed-rank test: nasal versus temporal hemifield or superior versus inferior hemifield.

Similarly to the second-order kernel response in both groups, in the first-order kernel response, the summed amplitude in the superior hemisphere was smaller than that in the inferior hemisphere, and the summed amplitudes of the central 5° and 10°, but not that of the central 15°, were smaller in the nasal hemisphere than in the temporal hemisphere. In the peak latencies, there were no hemispherical differences between the superior and inferior hemifields, or between nasal and temporal hemifields, for the three eccentricities in both glaucoma groups.

Comparison of First- and Second-Order Kernels of mfERGs recorded from Concentric Rings in Controls and Glaucoma Patients

Comparison of the first-order kernel of controls and glaucomatous subjects with hemifield defects showed that there was no statistical difference in the amplitude from each hemisphere, or in the S/I or N/T amplitude ratios for the three eccentricities (Table 3; ANOVA). On the other hand, there was a significant prolongation of the trough latency of the central 10° in the nasal, temporal, and superior hemispheres, and in the nasal and superior 15° rings ($P = 0.030$, 0.022, 0.006, 0.019, and 0.027, respectively; ANOVA).

For the second-order kernel, the N/T amplitude ratio of the central 5° was significantly different from that of other eccentricities ($P = 0.0001$; ANOVA; Table 4). Additionally, there was a significant difference in the N/T amplitude ratio between the normal control group and in both the superior and inferior hemifield predominant groups (Fig. 6; $P = 0.0005$, 0.0012, respectively, Scheffé test). There was also a statistically significant prolongation of the trough latency of the response from the central 15° in the hemispheres ($P = 0.014$; ANOVA). The N/T amplitude ratio of the central 5° was the most sensitive parameter that distinguished normal controls from NTG patients.

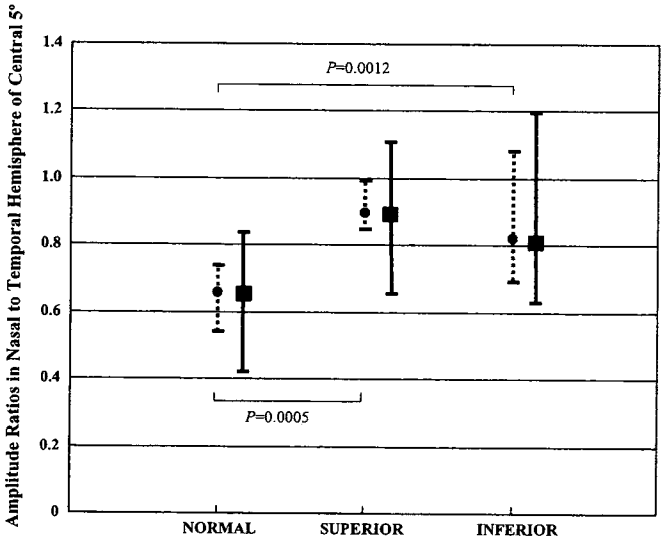

Figure 6. The nasal to temporal amplitude ratios of the central 5° differed significantly between the normal control group and the superior or inferior hemifield-predominant NTG groups. *Solid lines,* 97.5%–2.5%; broken lines, 75.0%–25%.

We calculated the receiver-operating characteristic (ROC) curve, which illustrates the sensitivity and specificity for discrimination of glaucomatous from normal eyes for different cutoff levels for the amplitude of the N/T amplitude ratios of the central 5°. The area under the ROC curve was 0.86. With a cutoff value of 0.83, the sensitivity was 65% and the specificity was 96.7%.

Correlation between the N/T Amplitude Ratio and Static Perimetric Findings

Our calculations showed that the correlations between the N/T amplitude ratio of the first-order kernel with the point

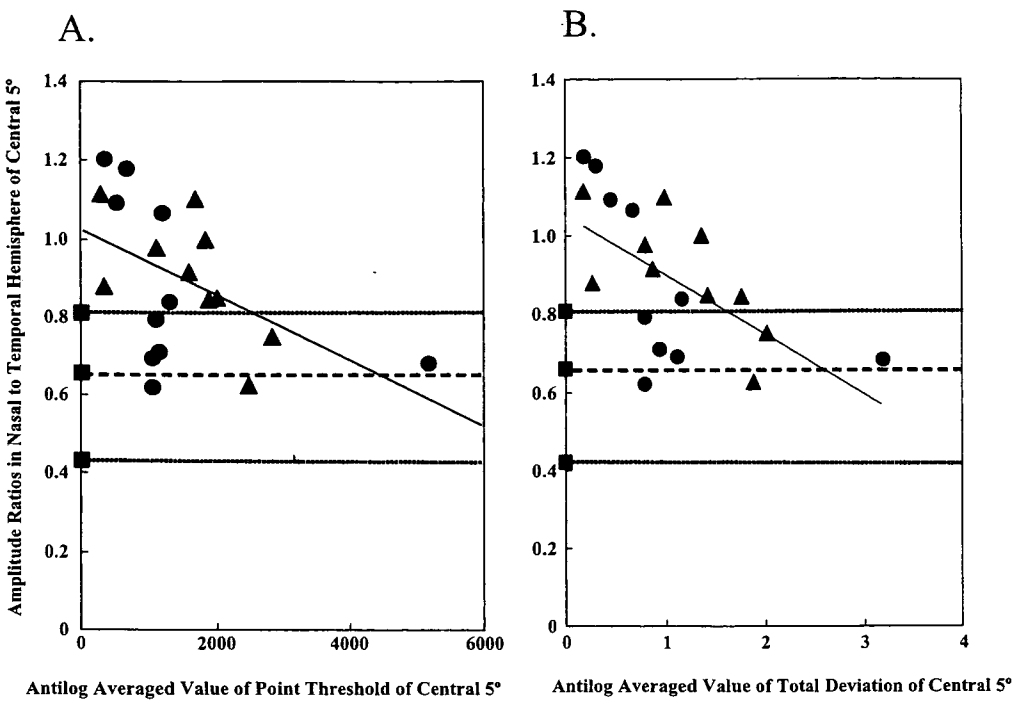

Figure 7. Relationships between nasal to temporal (N/T) amplitude ratio in the second-order kernel and the antilog averaged value of the point threshold (**A**) or of total deviation (**B**) obtained by the Humphrey central 30-2 program in NTG patients. The N/T amplitude ratio of the central 5° was significantly correlated with the antilog averaged value of each parameter of the central 5° (point threshold, r_s = –0.4602, P = 0.0448; total deviation, r_s = –0.6556, P = 0.0042). N/T ratio: ▲, superior; ●, inferior; ■, 10th–90th percentile in normal patients.

threshold or with the total deviation obtained with the Humphrey central 30-2 program were not significant. In addition, although the correlation coefficient between the N/T amplitude ratio of the second-order kernel and the point threshold or total deviation obtained with the Humphrey central 30-2 program increased with larger visual field areas, the correlation was not significant. However, there was a significantly strong correlation between the N/T amplitude ratio in the second-order kernel and the antilog averaged value of each parameter obtained with the Humphrey program central 30-2 (point threshold, r_s = –0.4602, P = 0.045; total deviation, r_s = *0.0020.656, P = 0.004; Fig. 7). A plot of the N/T amplitude ratio in the central 5° showed that 13 of 20 NTG patients were outside the 10th–90th percentile limits of the control group (Fig. 7; mean, 0.65; range of the 10th–90th percentiles, 0.44–0.81). Of these 13 NTG patients, eight had a superior hemisphere-dominant defect.

Discussion

Our results showed that mfERGs can be used to provide useful indices for detecting the presence of glaucomatous optic neuropathy. In particular, the second-order kernel response of the mfERGs within the central 5° can be used as a measure of retinal function in glaucomatous optic neuropathy. The value of this parameter was outside the 10th to 90th percentile range in 65% of NTG patients. The N/T amplitude ratio provided a good index for discriminating between individuals of the NTG and control groups.

Fortune et al.[16] reported that the area under the ROC curve of the amplitude of the oscillatory component in glaucoma patients was 0.88. The area under the ROC curve of the N/T amplitude ratio in our study was 0.86, and thus has approximately the same capability to discriminate between NTG patients and normal subjects.[16]

The mean refractive error in the NTG group was significantly higher than that in the normal group. Kawabata and Adachi-Usami[18] reported that the amplitudes of the first-order kernel of the mfERG were reduced and latencies were delayed in eyes with higher refractive errors. However, as shown in Tables 3 and 4, the amplitudes of the first- and second-order kernels of the NTG group were not significantly smaller than those of the normal group. Using the N/T ratio as the index should decrease the effect of refractive errors.

Hasegawa et al.[10] reported that the peak latencies of P1 and N2 of the first-order kernels in eyes with primary open-angle glaucoma (POAG) were significantly prolonged compared with those in normal eyes, although the differences in the amplitudes of (P1-N1) and (P1-N2) were not significantly different in the two groups. In this study, we demonstrated that there was no hemispherical difference in the amplitudes or the trough latency of the first-order kernel components of mfERGs in either the superior or inferior hemifield-predominant groups. These findings suggest that the first-order kernel components of the mfERG do not provide a good measure of the function of RGCs.

On the other hand, the second-order kernels are mainly attributable to components originating from the inner retinal layer.[19] An algorithm to extract the ONHC has been determined. The latency of this component increases as a function of the distance from the optic nerve head.[6] Bearse et al.[5] reported that the waveform of the second-order kernel had a nasal–temporal symmetry in glaucomatous

Jpn J Ophthalmol
Vol 51: 379–389, 2007

eyes compared with in normal eyes, suggesting that these waveforms might reflect a decrease in surviving RGCs throughout the retina in glaucomatous eyes. In addition, Fortune et al.[16] reported a selective loss of the oscillatory potentials of the first-order kernel from the temporal retina in eyes with POAG. They suggested that this was not only related to abnormalities in the inner plexiform layer in the temporal region but also was partly due to alterations of the ONHC. Kamei and Nagasaka[20] reported that the loss of nasal–temporal asymmetry in the second-order kernel response within the central 5° in eyes with optic disc atrophy might be attributable to RGC dysfunction. However, other investigators[21] reported that components of the second-order kernel were not correlated with glaucomatous visual field changes at early stages of glaucoma, suggesting that these components did not represent RGC function.

In previous analyses using quadrants[14,22] or eccentric groups[8] over the wider visual fields, or all traces over the entire visual field,[9,14] independent components of the mfERGs might have been superimposed on the ONHC, resulting in smaller and more subtle changes in the mfERGs. Even in our study with the averaging of relatively small areas, comparisons between glaucomatous eyes with superior and inferior-dominant hemifield defects showed no statistical difference in the amplitudes, S/I amplitude ratios of the superior to inferior hemispheres, or trough latencies of the second-order kernels.

However, in the comparison of temporal and nasal hemifields within the central 5°, there was a statistical difference in the N/T amplitude ratio between normal volunteers and glaucoma patients, and there was a loss of nasal–temporal asymmetry in glaucoma patients. A loss of the nasal–temporal asymmetry in glaucoma patients has already been reported.[5,6,14–16] Nasal–temporal asymmetry in normal subjects was first described by Sutter and Bearse,[6] who reported it to be elicited in the second-order kernel response of the mfERG under high contrast and fast flicker stimulus conditions. When the number of stimulus elements was 103, the contrast was 98%, and maximum luminance was 600 cd/m^2 with a natural pupil.[6] Thereafter, this phenomenon was also investigated using different stimulus settings such as low-contrast or global flash stimuli.[14–16] We used high initial contrast and fast flicker stimulus conditions, based on the report by Sutter and Bearse,[6] except we used 37 stimulus elements and a maximum luminance of 200 cd/m^2 with a dilated pupil for easy recording and analysis.

Sutter and Bearse[6] also reported that the spatial distribution of the ONHC is higher in the central fields. In the current study, there was a statistically significant difference in the N/T amplitude ratio within the central 5° between NTG patients and normal volunteers, but not in that within the central 10° or 15°. Considering that even within the central 5°, there was no significant difference in the amplitudes between the two groups, the amplitude ratio is useful for decreasing interindividual variations. The amplitudes of the second-order kernel response in the nasal hemisphere within the central 5° in glaucoma patients were larger than those in normal volunteers. We also noticed that in some patients, the N/T amplitude ratios of the second-order kernel were >1.0, and that these values were close to the N/T amplitude ratio of the first-order kernel in normal eyes. Assuming that the second-order kernel of the mfERGs results from contributions of a retinal component and the ONHC,[6] we suggest that in normal subjects these two components had antagonistic effects, whereas in glaucoma patients they did not, because the ONHC is smaller.

We showed that the N/T asymmetry of amplitude of the second-order kernel was inversely correlated with visual field threshold deviation locally and widely. Kato and colleagues[23] showed that in eyes with NTG with hemifield visual defects, a significant correlation existed between Heidelberg retina tomographic parameters and visual field indices in the unaffected hemifields. Similarly, in a frequency-doubling perimetric study,[17] visual field abnormalities, even in the intact hemifield in some NTG eyes with upper or lower hemifield defects, were determined by conventional differential light sensitivity perimetry with a Humphrey field analyzer. Moreover, Thienprasiddhi et al.[24] found that the multifocal visual evoked potential technique might detect functional damage at an earlier stage of glaucoma than traditional automated perimetry. Therefore, the strong correlation between the decrease in N/T asymmetry in glaucomatous eyes and visual field indices might suggest disturbances in the entire visual field even at the earlier stages of glaucoma.

In conclusion, we demonstrated that the second-order kernels of mfERGs largely reflected functions of the inner retinal layer, including those of RGCs. In addition, we showed a high and significant correlation between the N/T amplitude ratio of the second-order kernel and the antilog averaged value of the visual field point threshold and total deviation parameters. Our findings support the use of mfERGs for glaucoma patients. However, the current study was a cross-sectional study, and a prospective longitudinal intensive investigation of mfERGs, including determination of whether progression in glaucoma can affect the mfERG response, or whether loss of nasal–temporal asymmetry appears in early stages of glaucoma or ocular hypertension, is needed. Further study is required before our results can be applied in a clinical setting.

References

1. Minckler DS, Bunt AH, Johanson GW. Orthograde and retrograde axoplasmic transport during acute ocular hypertension in the monkey. Invest Ophthalmol Vis Sci 1977;16:426–441.
2. Ventura LM, Porciatti V, Ishida K, Feuer WJ, Parrish RK II. Pattern electroretinogram abnormality and glaucoma. Ophthalmology 2005;112:10–19.
3. Biersdorf WR. The foveal electroretinogram is normal in optic atrophy. Doc Ophthalmol Proc Ser 1984;40:127–135.
4. Jacobson SG, Sandberg MA, Effron MH, Berson EL. Foveal cone electroretinograms in strabismic amblyopia: comparison with juvenile macular degeneration, macular scars, and optic atrophy. Trans Ophthalmol Soc U K 1979;99:353–356.
5. Bearse, MA, Sutter EE, Sim D, Stamper R. Glaucomatous dysfunction revealed in higher order components of the electrogram.

In: Vision science and its applications, 1996 OSA Technical Digest Series, Vol. 1. Washington, D.C: Optical Society of America; 1996. p. 104–107.
6. Sutter EE, Bearse MA. The optic nerve head component of the human ERG. Vision Res 1999;39:419–436.
7. Bearse MA Jr, Sutter EE. Imaging localized retinal dysfunction with the multifocal electroretinogram. J Opt Soc Am A Opt Image Sci Vis 1996;13:634–640.
8. Palmowski AM, Allgayer R, Heinemann-Venaleken B. The multifocal ERG in open angle glaucoma—a comparison of high and low contrast recordings in high- and low-tension open angle glaucoma. Doc Ophthalmol 2000;101:35–49.
9. Fortune B, Cioffi GA, Johnson CA, Kondo Y, Mochizuki K, Kitazawa Y. The relationship between multifocal electroretinography and standard automated perimetry findings in normal-tension glaucoma. In: Weinreb RN, Kitazawa Y, Krieglstein GK, editors. Glaucoma in the 21st century. London: Mosby International; 2000. p. 73–78.
10. Hasegawa S, Takagi M, Usui T, Takada R, Abe H. Waveform changes of the first-order multifocal electroretinogram in patients with glaucoma. Invest Ophthalmol Vis Sci 2000;41:1597–1603.
11. Palmowski AM, Allgayer R, Heinemann-Vernaleken B, Ruprecht KW. Multifocal electroretinogram with a multiflash stimulation technique in open-angle glaucoma. Ophthalmic Res 2002;34: 83–89.
12. Murai K, Tazawa Y, Kobayashi M, Hayasaka A. Amplitude of the s-wave of multifocal electroretinograms can indicate local retinal sensitivity in glaucomatous eyes. Jpn J Ophthalmol 2004;48: 215–221.
13. Miyake Y, Shiroyama N, Horiguchi M, Ota I. Asymmetry of focal ERG in human macular region. Invest Ophthalmol Vis Sci 1989;30:1743–1749.
14. Hood DC, Greenstein VC, Holopigian K, et al. An attempt to detect glaucomatous damage to the inner retina with the multifocal ERG. Invest Ophthalmol Vis Sci 2000;41:1570–1579.
15. Hood DC. Assessing retinal function with the multifocal technique. Prog Retinal Eye Res 2000;19:607–646.
16. Fortune B, Bearse Jr MA, Cioffi GA, Johnson CA. Selective loss of an oscillatory component from temporal retinal multifocal ERG responses in glaucoma. Invest Ophthalmol Vis Sci 2002;43: 2638–2647.
17. Kondo Y, Yamamoto T, Sato Y, Matsubara M, Kitazawa Y. A frequency-doubling perimetric study in normal-tension glaucoma with hemi-field defect. J Glaucoma 1998;7:261–265.
18. Kawabata H, Adachi-Usami E. Multifocal electroretinogram in myopia. Invest Ophthalmol Vis Sci 1997;38:2844–2851.
19. Horiguchi M, Suzuki S, Kondo M, Tanikawa A, Miyake Y. Effect of glutamate analogues and inhibitory neurotransmitters on the electroretinograms elicited by random sequence stimuli in rabbits. Invest Ophthalmol Vis Sci 1998;39:2171–2176.
20. Kamei A, Nagasaka E. Multifocal electroretinograms (ERG) and retinal nerve fiber layer thickness (RNFLT) in patients with damaged optic nerve with or without optic disc atrophy. In: Sharpe, J, editor. Neuro-ophthalmology at the beginning of the new millennium. Englewood, NJ: Medimond Medical Publications; 2000. p. 17–22.
21. Sakemi F, Yoshii M, Okisaka S. Multifocal electroretinograms in early primary open-angle glaucoma. Jpn J Ophthalmol 2002;46: 443–450.
22. Palmowski AM, Ruprecht KW: Follow up in open angle glaucoma. A comparison of static perimetry and the fast stimulation mfERG. Doc Ophthalmol 2004;108:55–60.
23. Kato A, Tomita G, Kono Y, Kitazawa Y. Relation between visual field indices and optic disc cupping in normal-tension glaucoma with hemi-field visual defects. Atarashii Ganka (J Eye) 1997;14: 921–923.
24. Thienprasiddhi P, Greenstein VC, Chen CS, Liebmann JM, Ritch R, Hood DC. Multifocal visual evoked potential responses in glaucoma patients with unilateral hemifield defects. Am J Ophthalmol 2003;136:34–40.